Mechanical rotation modifies the manifestation of photon entanglement

Marion Cromb, Sara Restuccia, Graham M. Gibson, Marko Toroš ⬤, Miles J. Padgett,[*] and Daniele Faccio[†]
School of Physics and Astronomy, University of Glasgow, Glasgow G12 8QQ, United Kingdom

Mechanical rotation plays a central role in fundamental physics theories and has profound connections with the theory of general relativity. However, very few experiments have so far aimed to explore the interplay of mechanical rotation with entangled photon states. By adding Sagnac interferometers into the arms of a Hong-Ou-Mandel (HOM) interferometer that is placed on a mechanically rotating platform, we experimentally observe the modification of the symmetry of an entangled biphoton state due to noninertial motion. As the platform rotation speed is increased, we observe that HOM interference dips transform into HOM interference peaks. This indicates that the photons pass from perfectly indistinguishable (bosonic behavior), to perfectly distinguishable (fermionic behavior). This demonstration is of relevance to global satellite quantum communications and paves the way for further fundamental research that can test the influence of curved space on quantum entanglement.

Introduction. Mechanical rotations play an important role in fundamental research [1]. They can be measured using a Sagnac interferometer in which two counterpropagating light beams follow a closed-loop path [2,3]. Such an interferometer relies on the Sagnac effect, a genuinely relativistic effect, which emerges from the proper-time difference between the two beams completing the loop [4–7]. The Sagnac effect has also been investigated in the general relativistic context, connecting it to the rotating Kerr spacetime and the equivalence principle [8–13]. It forms the basis for ring laser gyroscopes which can achieve exquisite sensitivities [14,15], and efforts are underway to test the Lense-Thirring frame-dragging effect induced by the Earth's rotation [16,17]. Furthermore, modified interferometers could constrain alternative theories of gravity [18–21], test the interface of quantum mechanics and gravity [22–25], and sense gravitational waves [26–29].

Recent research has started to experimentally test photonic quantum entanglement in noninertial frames. Fink *et al.* were able to place a bound on the (non)effect of uniform acceleration on the amount of entanglement up to 30 g in a centrifuge [30]. Related experiments demonstrated a gyroscope that uses path-entangled NOON states to provide superresolution and Sagnac phase sensitivity beyond the shot-noise limit [31], providing an indication that mechanical rotations can affect measurements of entangled states. Noninertial rotational motion was also shown to influence the temporal distinguishability of photons, as measured through Hong-Ou-Mandel (HOM) interference [32].

Here, we report an experiment where noninertial motion directly modifies how entanglement manifests itself in a two-photon interferometer that is placed in rotation. This experiment builds upon previous theoretical predictions [33] and provides experimental evidence of an interaction between mechanical rotation and quantum entanglement. By altering the rotation speed of a modified HOM interferometer, we are able to change a Hong-Ou-Mandel interference dip into a peak, antisymmetrizing the entangled state and changing bosonic photon behavior into "fermionic" behavior. This result has no classical analog, can only occur with entangled states, and thus unequivocally shows that the manifestation of entanglement is affected already by low-frequency mechanical rotations.

Hong-Ou-Mandel interference. Hong-Ou-Mandel (HOM) biphoton interference [34] provides information about the distinguishability of photons. When two independent single photons cross at a lossless 50:50 beam splitter, the unitarity of the beam-splitter transformation, combined with the photon bosonic commutation relations, results in an interference forcing indistinguishable photons to "bunch" and exit the beam splitter through the same port. A time delay between the input photons creates distinguishability between the photons. Counting coincident detections between single-photon detectors in the two output paths, a dip in the coincidence rate is observed when the photons temporally overlap. The visibility of the dip indicates overall indistinguishability in all photon properties.

In an analogous experiment with fermions, the fermionic anticommutation relations would suppress the bunching of independent fermions and a peak in the output coincidences would be observed instead. This "fermionic" behavior can also be observed with bosons if and only if the particles are entangled in an antisymmetric state [35–37], which can be engineered in a number of ways [38–46]. In this way, a HOM peak acts as a witness for (antisymmetric) entanglement.
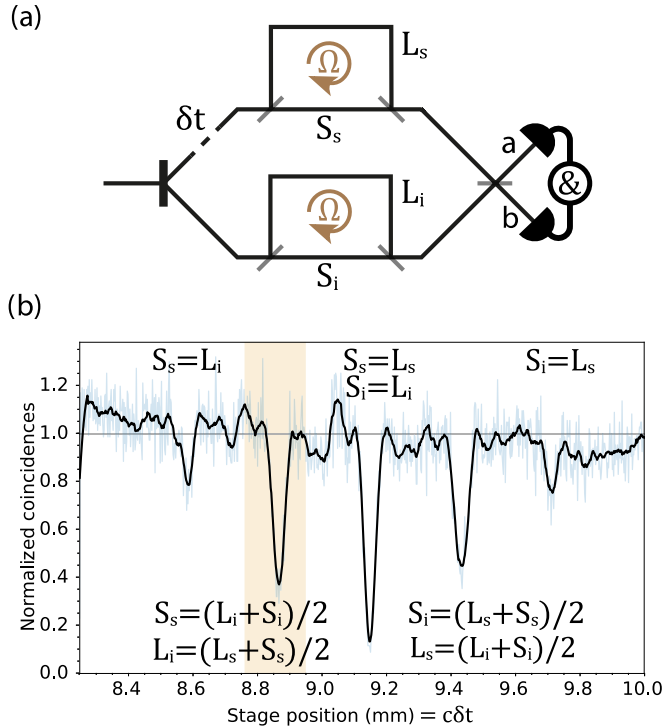
*miles.padgett@glasgow.ac.uk
†daniele.faccio@glasgow.ac.uk

(a)

(b)

FIG. 1. (a) Schematic layout. Figurative diagram showing short S and long L path lengths (which travel against and with the rotation Ω direction) for the signal and idler photons in the system, along with the HOM delay δt that scans the delay of one arm with respect to the other, and the detection in coincidence after the HOM beam splitter. (b) Experimental scan of dips while not rotating. A graph of detected coincidences against the position of the stage, which is proportional to the HOM delay δt. Raw experimental data are shown in light blue, with a smoothed average in black. Each point was acquired for 5 s with an average background count (normalized to 1 in the figure) of 30 coincidences/s. Five dips in the coincidences are present, corresponding to the different combinations of path lengths S_s, L_i, etc., at which HOM interference can occur. The shaded region shows an example range over which the stage is scanned when the experiment is in rotation.

Outline of the experiment. A schematic of the rotating Hong-Ou-Mandel (HOM) interferometer is shown in Fig. 1(a). A pair of indistinguishable time-frequency entangled photons are produced in a nonlinear crystal and travel in separate arms [denoted with index s (i), indicating the signal (idler) photon] until interfering at a final beam splitter, after which they are detected in coincidence. In each of the arms, each photon is also split 50:50 into two directions, taking either a long path ($L_{\{s,i\}}$) traveling clockwise, or a short path ($S_{\{s,i\}}$) traveling anticlockwise. The extra paths are set so that the arms are symmetric, $L_s - S_s = L_i - S_i$. A variable overall delay δt is also added into the signal arm, which varies both S_s and L_s equally. There are three different settings of the overall delay at which photons cross the beam splitter at the same time: when $S_s = L_i$, when $L_s = S_i$, and when both $L_s = L_i$, $S_s = S_i$. The various combinations of the extra paths therefore result in additional HOM dips in the coincidence measurements at different delays δt.

If the input light is entangled (rather than being two independent single photons), two additional interference

features appear between these dips. These correspond to the delays at which $S_s = (L_i + S_i)/2$, $L_i = (L_s + S_s)/2$ and $L_s = (L_i + S_i)/2$, $S_i = (L_s + S_s)/2$. These additional interference features can be dips, but depending on the modulo 2π phase between paths S and L, they can disappear completely, or can flip to become peaks [41–46].

The experiment is mounted on a rotating table. When the experiment is put into rotation at angular frequency Ω, the Sagnac effect changes the time it takes for light to travel with, or against the rotation direction by

$$\Delta t_{\mathrm{Sagnac}} = \frac{4A\Omega}{c^2}. \quad (1)$$

Although the path lengths S and L are fixed, when rotating the Sagnac time delay changes the phase difference between them, scaling with the area A enclosed by the paths. Increasing the rotation frequency so that the Sagnac phase difference between S and L paths increases by π is therefore expected to flip these interferences from dips to peaks or vice versa, altering the entanglement symmetry and changing the indistinguishability of the photons as measured by the HOM—purely through noninertial motion.

Theoretical model. We follow a similar approach to Ref. [43], here extended to account for the specific nature of the Sagnac interferometer and incorporating mechanical rotation. For our input state we assume degenerate type-I spontaneous parametric down-conversion (SPDC) pumped by frequency ω_p and add a variable delay δt between the signal and idler photon arms,

$$|\psi\rangle = \int_0^{\omega_p} d\omega B(\omega)e^{-i\omega\delta t}a_i^\dagger(\omega)a_s^\dagger(\omega_p - \omega)|0\rangle, \quad (2)$$

where $a_i^\dagger(\omega)$, $a_s^\dagger(\omega_p - \omega)$ are the creation operators for modes of frequency ω, $\omega_p - \omega$ for idler and signal photons, and $B(\omega)$ is the spectrum of the biphoton wave packet.

Each arm contains a nested fiber Sagnac interferometer where the light hits a beam splitter, splits into clockwise (CW) and anticlockwise (ACW) directions, propagates in opposite directions through the same fiber loop of radius r for time $t_{\{CW, ACW\}}$, and recombines when it hits the beam splitter again upon exiting the nested Sagnac interferometer,

$$a_i^\dagger(\omega) \mapsto \frac{1}{2}\left(e^{-i\omega t_{i,CW}} - e^{-i\omega t_{i,ACW}}\right)a_{i,\mathrm{out}}^\dagger(\omega)$$
$$+ \frac{i}{2}\left(e^{-i\omega t_{i,CW}} + e^{-i\omega t_{i,ACW}}\right)a_{i,\mathrm{back}}^\dagger(\omega). \quad (3)$$

As well as the Sagnac delay created between clockwise and anticlockwise photons traveling in a total fiber length L_f, the polarization maintaining fiber paths are constructed such that there is an additional constant birefringent delay from a mismatch between refractive indices n_{CW} and n_{ACW} over a length $L_b \ll L_f$ (see Fig. 2). This extra net delay is independent of rotation and creates the short S and long L paths in Fig. 1(a) schematic, ensuring separation into a total of five interference features shown in Fig. 1(b). The total time delays are thus

$$t_{CW}(\Omega) = \frac{L_b n_{CW}}{c} + \frac{L_f r\Omega}{c^2},$$
$$t_{ACW}(\Omega) = \frac{L_b n_{ACW}}{c} - \frac{L_f r\Omega}{c^2}. \quad (4)$$
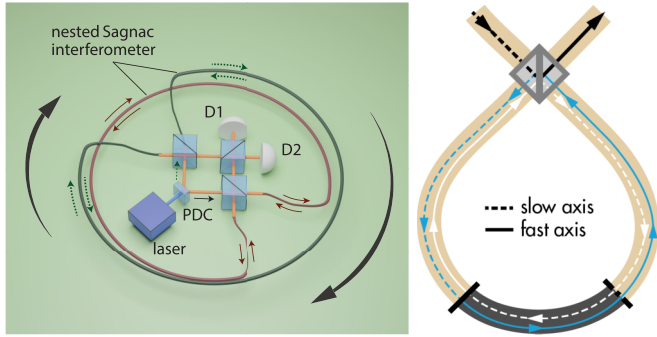
FIG. 2. Diagram of experiment. Left: Rotating Hong-Ou-Mandel experiment with nested Sagnac interferometers that enclose the area of the rotating platform. A pump laser produces photon pairs at a nonlinear crystal (PDC indicates the crystal followed by a filter that blocks the pump laser and a knife-edge prism that separates the two photons) which each pass through a Sagnac interferometer and then interfere at a beam splitter. D1 and D2 are two single-photon detectors which can measure in coincidence. Right: Detail of the 1 m birefringent delay between clockwise and anticlockwise directions created by the fiber loop in the nested Sagnac interferometers. This makes the HOM peaks easier to observe as a birefringent delay larger than the single-photon coherence length ensures a consistent amount of light passing through the Sagnacs. Two 20-m polarization-maintaining fibers are connected by a hybrid 1-m patch cord that flips the polarization axis, so one direction in the Sagnac loop has 21 m of slow axis and 20 m of fast axis, and the other has 21 m of fast axis and 20 m of slow axis.

Here, we assume that L_f, L_b, and r are the same for signal and idler and thus $t_{i,\mathrm{CW}} = t_{s,\mathrm{CW}} = t_{\mathrm{CW}}$ and $t_{i,\mathrm{ACW}} = t_{s,\mathrm{ACW}} = t_{\mathrm{ACW}}$ (for a more general approach, see Supplemental Material [47]).

The light that exits the Sagnacs $(a_{i,\mathrm{out}}, a_{s,\mathrm{out}})$ interferes at the HOM beam splitter; at its outputs (a, b) we find the final state:

$$|\psi_{\mathrm{final}}\rangle = \frac{1}{8} \int_0^{\omega_p} d\omega B(\omega) e^{-i\omega \delta t} \left(e^{-i\omega t_{\mathrm{CW}}} - e^{-i\omega t_{\mathrm{ACW}}} \right)$$
$$\times \left(e^{-i(\omega_p - \omega)t_{\mathrm{CW}}} - e^{-i(\omega_p - \omega)t_{\mathrm{ACW}}} \right) [ia^\dagger(\omega) + b^\dagger(\omega)]$$
$$\times [a^\dagger(\omega_p - \omega) + ib^\dagger(\omega_p - \omega)]|0\rangle. \quad (5)$$

The expected coincidences N_c, measured between two single-photon detectors in the output arms, is calculated (details given in Supplemental Material [47]). Assuming a Gaussian spectrum for $B(\omega)$ of characteristic width $\Delta\omega$ we find

$$N_c \propto C_b - e^{-\Delta\omega^2(\delta t + \Delta t)^2} - e^{-\Delta\omega^2(\delta t - \Delta t)^2}$$
$$+ 4\cos\left(\frac{\omega_p}{2}\Delta t\right)\left(e^{-\Delta\omega^2\left(\delta t + \frac{\Delta t}{2}\right)^2} + e^{-\Delta\omega^2\left(\delta t - \frac{\Delta t}{2}\right)^2} \right)$$
$$- 4e^{-\Delta\omega^2\delta t^2} - 2\cos(\omega_p\Delta t)e^{-\Delta\omega^2\delta t^2}, \quad (6)$$

where $\Delta t = t_{\mathrm{CW}} - t_{\mathrm{ACW}}$. Equation (6) contains a first term that does not depend on the HOM delay δt and that forms the coincidence background:

$$C_b = 4 - 8e^{-\frac{\Delta\omega^2}{4}(\Delta t)^2}\cos\left(\frac{\omega_p}{2}\Delta t\right)$$
$$+ 2\cos(\omega_p\Delta t) + 2e^{-\Delta\omega^2(\Delta t)^2}. \quad (7)$$

Of the terms in Eq. (6) that depend on δt and describe interference features, three describe "fixed" HOM dips: a central dip and two smaller dips either side (second, third, and fifth terms). There are then oscillating terms, two of which describe two fully oscillating dips/peaks in between the central fixed dip and side dips (fourth term comprising the whole second line), and another which can increase the depth of the central dip (sixth term, essentially ensuring the central dip remains fully visible when the light is fully indistinguishable even as the background C_b fluctuates). From the periodicity of the fully oscillating dips [the $\cos\left(\frac{\omega_p}{2}\Delta t\right)$ term] we find that a change in rotation frequency of $c\lambda_p/(4\pi L_f r)$ Hz can fully flip a dip into a peak. It is this flip from a dip to a peak that is direct evidence of a change in behavior from bosonic to fermionic.

Experimental apparatus. The experiment shown in Fig. 2 is mounted on a rotating table driven by a stepper motor (RS-PRO, 180-5292) run by a controller module (Geckodrive, G201X). A UV pump laser (355 nm, Coherent Genesis CX STM) produces degenerate down-converted (PDC) photon pairs ($\lambda = 710$ nm) at a type-I beta barium borate (BBO) crystal. These (symmetrically) frequency-entangled photons are separated using a knife-edge prism, filtered (10 nm bandwidth), and each coupled into a polarization maintaining fiber (PMF). One fiber coupler is mounted on a translation stage in order to scan the temporal delay δt. Each fiber arm contains a nested Sagnac interferometer, consisting of a beam splitter with its reflection and transmission ports connected by a 41-m loop of PMF. This optical fiber link is secured around the rotating platform in loops of diameter 0.908 m. The 41-m fiber link is made up of three fiber optic cables connected in series: two 20 m lengths with a 1-m fiber in the middle which has one key aligned to the slow axis and the other key aligned to the fast axis (shown in Fig. 2). This 1-m fiber flips the polarization axis as the light travels around, creating a fixed net 1 m birefringent delay (beat length ~ 1.1 mm) between light traveling in different directions around the loop, creating short and long path options. As the two Sagnac interferometers do not share the same optical fiber, any temperature fluctuations affecting one fiber and not the other can introduce unwanted noise. To minimize these issues, the two Sagnac fibres are looped alongside each other and thermally insulated. After the Sagnac interferometers, the light in each arm recombines at a final HOM beam splitter and the photons at the outputs are detected by single-photon avalanche diodes (SPADs, D1 and D2 in Fig. 2) which measure singles and coincidences within a coincidence window of 5 ns.

Measuring coincidences while scanning the delay δt resulted in the series of five HOM dips [shown in Fig. 1(b)] as expected from the different paths in the system and cross interference between the paths.

When the setup is rotated at a constant speed, the Sagnac effect causes an additional phase shift between light traveling clockwise and anticlockwise around the loops, and with a large enough change in rotation speed this additional phase shift changes the symmetry of the entangled biphoton state such that the cross-interference features can flip from a dip to a peak and vice versa.
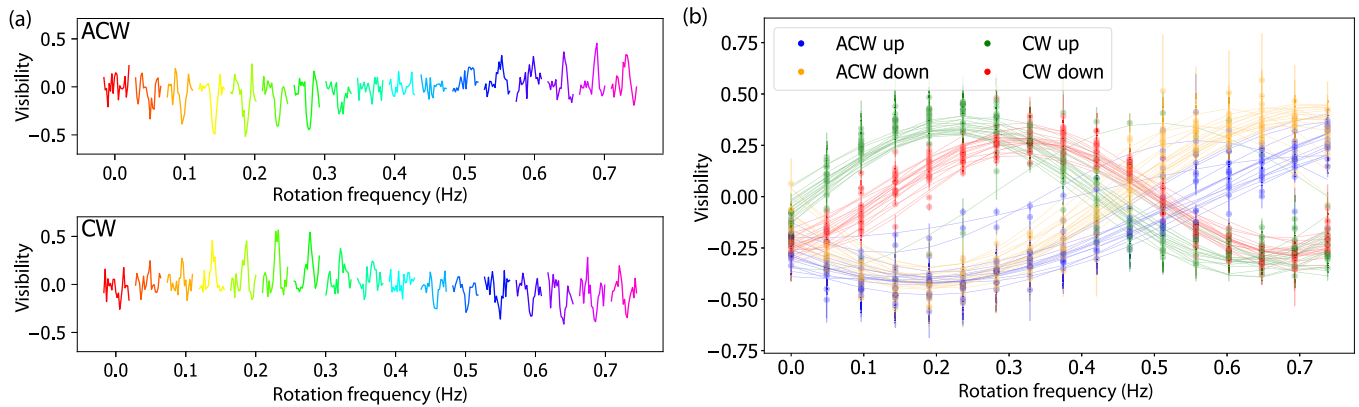
FIG. 3. (a) Dips inverting for clockwise and anticlockwise rotations. Each individual curve, marked in a different color, is a short, 0.2 mm delay scan around the peak [see shaded region in Fig. 1(b)] at a single rotation frequency. The peak scans are ordered on the graph by the rotation frequencies (from 0 to 0.735 Hz) as indicated on the horizontal axis. Contrasts adjacent clockwise (CW) and anticlockwise (ACW) runs, to show how the effect depends on direction, consistent with the Sagnac effect. (b) Interference peak values with increasing rotation speed. Data from a long overnight measurement run (~80 sequences). Plots peak height over background for each rotation speed (dots) and the best fit sinusoids for each 0–0.74 Hz ("up") or 0.74–0 Hz ("down") sequence. Each sequence took ~10 min. It is clear that clockwise and anticlockwise rotations move the peak in opposite directions from a similar starting phase.

The rotation speed of the apparatus was changed from 0 Hz to a maximum rotation speed (~0.735 Hz) in equally set steps (see Supplemental Material for more information [47]). It was then stepped back down again to 0 Hz. These sequences were repeated, alternating between rotating anticlockwise and clockwise. The maximum speed was set conservatively to ensure the experiment could be repeated consistently over several hours without damage to the equipment or changes to the alignment due to vibrations at higher rotation speeds.

At each rotation speed, the delay stage was used to scan over the second dip from the left [the shaded region in Fig. 1(b)] in equal steps. The singles and coincidences were measured at each delay stage position for a short acquisition time. Most of the data were taken with a 10 μm step size and a 1.5 s acquisition time. Background coincidence rates for these measurements were of the order 100 counts/s.

Results. The results in Fig. 3 clearly show that the rotation changed the biphoton state as predicted and that the HOM interference changed smoothly and sinusoidally from a dip to a peak and vice versa as the rotation was stepped up or down. Depending on whether the experiment is spinning clockwise or anticlockwise, the Sagnac effect will either increase the phase between the nested paths or decrease it. As such, we expect that if we start from neither a dip nor a peak then rotating the experiment in one direction will turn it to a peak first as rotation speed increases, and the other direction will turn into a dip first as rotation speed increases. This can be seen in the experimental data (Fig. 3). This dependence on rotation direction confirms that the main observed effect is due to the predicted Sagnac effect and is not due to spurious effects caused by centrifugal forces on the setup, which would not be dependent on the sense of rotation.

As the experiment consists of many meters of optical fiber, it was also sensitive to temperature changes [48] from the laboratory environment and from the operation of the electronics and the motor in the experiment. These temperature changes added extra phase drifts that changed over time, and

thus also altered across measurement sequences precisely how many rotation steps were required to see a flip of the dip. To reduce these temperature noise effects, the measurements were performed in short time intervals while retaining an acceptable signal-to-noise ratio. We then averaged over 151 individual rotation sequences in order to average out small random changes and fluctuations in the environment. Some difference in periodicity might be anticipated between the clockwise and anticlockwise directions due to the g-force on the fibers mentioned above, creating a common phase offset that in one direction works with, and in the other against, the Sagnac effect. Indeed, the mean of the 78 clockwise measurements was 0.41 Hz, and the mean of the 73 anticlockwise measurements was 0.53 Hz. Overall, averaging across all data, we measured a dip-to-peak rotation change (half period) of mean $0.47^{+0.10}_{-0.11}$ Hz, and median 0.43 Hz, that matched well our theoretical expected value of 0.455 Hz.

Conclusions. We have shown that the statistics of biphoton interference can change depending on the noninertial motion of the experimental frame. Noninertial motion modifies the entanglement symmetry of the input biphoton state such that we observe Hong-Ou-Mandel interference dips ("bosonic" behavior) change into peaks ("fermionic" behavior) and vice versa, with changes in rotation speed of the setup. This experimental change is consistent with the magnitude and directionality of the Sagnac effect mechanism at the heart of our theoretical model. The dips that show this change do not appear in our simulations if we use two independent identical single photons as input; the mechanism for changing photon statistics acts on the frequency correlations between the photons that arise from the time-frequency entanglement of the photon pair.

This work shows the promising utility of combining photonic technologies and noninertial motion for testing fundamental physics questions at the interface of quantum mechanics and curved space. Taking these ideas and techniques further, it could be possible to create entanglement with rotational motion [25] or with other forms of noninertial

motion, particularly with nonuniform acceleration as indicated by theoretical research into quantum field theories in curved spacetimes [49–51].

All data used for the figures presented in this Letter are available online [52].

[1] A. Pais *"Subtle is the Lord…": The Science and the Life of Albert Einstein* (Oxford University Press, Oxford, U.K, 2008).

[2] G. Sagnac, L'éther lumineux démontré par l'effet du vent relatif d'éther dans un interféromètre en rotation uniforme', C.R. Acad. Hebd. Seances Sci. **157**, 708 (1913).

[3] G. Sagnac, Sur la preuve de la réalité de l'éther lumineux par l'expérience de l'interférographe tournant, C. R. Acad. Hebd. Seances Sci. **157**, 1410 (1913).

[4] E. J. Post, Sagnac effect, Rev. Mod. Phys. **39**, 475 (1967).

[5] H. J. Arditty and H. C. Lefèvre, Sagnac effect in fiber gyroscopes, Opt. Lett. **6**, 401 (1981).

[6] R. Anderson, H. R. Bilger, and G. E. Stedman, "Sagnac" effect: A century of Earth-rotated interferometers, Am. J. Phys. **62**, 975 (1994).

[7] G. B. Malykin, The Sagnac effect: correct and incorrect explanations, Phys. Usp. **43**, 1229 (2000).

[8] A. Ashtekar and A. Magnon, The Sagnac effect in general relativity, J. Math. Phys. **16**, 341 (1975).

[9] J. Anandan, Sagnac effect in relativistic and nonrelativistic physics, Phys. Rev. D **24**, 338 (1981).

[10] A. Tartaglia, General relativistic corrections to the Sagnac effect, Phys. Rev. D **58**, 064009 (1998).

[11] J. Frauendiener, Notes on the Sagnac effect in general relativity, Gen. Relativ. Gravit. **50**, 147 (2018).

[12] E. Benedetto, F. Feleppa, I. Licata, H. Moradpour, and C. Corda, On the general relativistic framework of the Sagnac effect, Eur. Phys. J. C **79**, 187 (2019).

[13] S. P. Kish and T. C. Ralph, Quantum effects in rotating reference frames, AVS Quantum Sci. **4**, 011401 (2022).

[14] A. D. Di Virgilio, C. Altucci, F. Bajardi, A. Basti, N. Beverini, S. Capozziello, G. Carelli, D. Ciampini, F. Fuso, U. Giacomelli *et al.*, Sensitivity limit investigation of a Sagnac gyroscope through linear regression analysis, Eur. Phys. J. C **81**, 400 (2021).

[15] A. D. V. Di Virgilio, F. Bajardi, A. Basti, N. Beverini, G. Carelli, D. Ciampini, G. Di Somma, F. Fuso, E. Maccioni, P. Marsili, A. Ortolan, A. Porzio, and D. Vitali, Sub-shot-noise sensitivity in a ring laser gyroscope, arXiv:2301.01386.

[16] F. Bosi, G. Cella, A. DiVirgilio, A. Ortolan, A. Porzio, S. Solimeno, M. Cerdonio, J. P. Zendri, M. Allegrini, J. Belfi, N. Beverini, B. Bouhadef, G. Carelli, I. Ferrante, E. Maccioni, R. Passaquieti, F. Stefani, M. L. Ruggiero, A. Tartaglia, K. U. Schreiber, A. Gebauer, and J. P. R. Wells, Measuring gravitomagnetic effects by a multi-ring-laser gyroscope, Phys. Rev. D **84**, 122002 (2011).

[17] A. D. V. Di Virgilio, J. Belfi, W.-T. Ni, N. Beverini, G. Carelli, E. Maccioni, and A. Porzio, Ginger: A feasibility study, Eur. Phys. J. Plus **132**, 157 (2017).

[18] K. K. Nandi, P. M. Alsing, J. C. Evans, and T. B. Nayak, Brans-Dicke corrections to the gravitational Sagnac effect, Phys. Rev. D **63**, 084027 (2001).

[19] J. Sultana, The Sagnac effect in conformal Weyl gravity, Gen. Relativ. Gravit. **46**, 1710 (2014).

[20] R. Kh. Karimov, R. N. Izmailov, A. A. Potapov, and K. K. Nandi, Terrestrial Sagnac delay constraining modified gravity models, Gen. Relativ. Gravit. **50**, 44 (2018).

[21] S. Capozziello, C. Altucci, F. Bajardi, A. Basti, N. Beverini, G. Carelli, D. Ciampini, A. D. V. Di Virgilio, F. Fuso, U. Giacomelli *et al.*, Constraining theories of gravity by GINGER experiment, Eur. Phys. J. Plus **136**, 394 (2021).

[22] J. Kohlrus, D. E. Bruschi, J. Louko, and I. Fuentes, Quantum communications and quantum metrology in the spacetime of a rotating planet, EPJ Quantum Technol. **4**, 7 (2017).

[23] C. Marletto and V. Vedral, Sagnac interferometer and the quantum nature of gravity, J. Phys. Commun. **5**, 051001 (2021).

[24] R. Barzel, D. E. Bruschi, A. W. Schell, and C. Lämmerzahl, Observer dependence of photon bunching: The influence of the relativistic redshift on Hong-Ou-Mandel interference, Phys. Rev. D **105**, 105016 (2022).

[25] M. Toroš, M. Cromb, M. Paternostro, and D. Faccio, Generation of Entanglement from Mechanical Rotation, Phys. Rev. Lett. **129**, 260401 (2022).

[26] W. Barker, Effects of the circularly polarized beam of linearized gravitational waves, Classical Quantum Gravity **34**, 167001 (2017).

[27] S. Lacour, F. H. Vincent, M. Nowak, A. Le Tiec, V. Lapeyrere, L. David, P. Bourget, A. Kellerer, K. Jani, J. Martino *et al.*, SAGE: Finding IMBH in the black hole desert, Classical Quantum Gravity **36**, 195005 (2019).

[28] J. Bičák, J. Katz, T. Ledvinka, and D. Lynden-Bell, Effects of rotating gravitational waves, Phys. Rev. D **85**, 124003 (2012).

[29] J. Frauendiener, Gravitational waves and the Sagnac effect, Classical Quantum Gravity **37**, 05LT01 (2020).

[30] M. Fink, A. Rodriguez-Aramendia, J. Handsteiner, A. Ziarkash, F. Steinlechner, T. Scheidl, I. Fuentes, J. Pienaar, T. C. Ralph, and R. Ursin, Experimental test of photonic entanglement in accelerated reference frames, Nat. Commun. **8**, 15304 (2017).

[31] M. Fink, F. Steinlechner, J. Handsteiner, J. P. Dowling, T. Scheidl, and R. Ursin, Entanglement-enhanced optical gyroscope, New J. Phys. **21**, 053010 (2019).

[32] S. Restuccia, M. Toroš, G. M. Gibson, H. Ulbricht, D. Faccio, and M. J. Padgett, Photon Bunching in a Rotating Reference Frame, Phys. Rev. Lett. **123**, 110401 (2019).

[33] M. Toroš, S. Restuccia, G. M. Gibson, M. Cromb, H. Ulbricht, M. Padgett, and D. Faccio, Revealing and concealing entanglement with noninertial motion, Phys. Rev. A **101**, 043837 (2020).

[34] C. K. Hong, Z. Y. Ou, and L. Mandel, Measurement of Subpicosecond Time Intervals Between Two Photons by Interference, Phys. Rev. Lett. **59**, 2044 (1987).

[35] K. Wang and S. Zhu, Two-photon anti-coalescence interference: The signature of two-photon entanglement, Europhys. Lett. **64**, 22 (2003).

[36] K. Wang, Quantum theory of two-photon wavepacket interfer-

ence in a beamsplitter, J. Phys. B: At., Mol. Opt. Phys. **39**, R293 (2006).

[37] A. Fedrizzi, T. Herbst, M. Aspelmeyer, M. Barbieri, T. Jennewein, and A. Zeilinger, Anti-symmetrization reveals hidden entanglement, New J. Phys. **11**, 103052 (2009).

[38] T. B. Pittman, D. V. Strekalov, A. Migdall, M. H. Rubin, A. V. Sergienko, and Y. H. Shih, Can Two-Photon Interference be Considered the Interference of Two Photons? Phys. Rev. Lett. **77**, 1917 (1996).

[39] P. G. Kwiat, A. M. Steinberg, and R. Y. Chiao, Observation of a "quantum eraser": A revival of coherence in a two-photon interference experiment, Phys. Rev. A **45**, 7729 (1992).

[40] S. P. Walborn, A. N. de Oliveira, S. Pádua, and C. H. Monken, Multimode Hong-Ou-Mandel Interference, Phys. Rev. Lett. **90**, 143601 (2003).

[41] D. V. Strekalov, T. B. Pittman, and Y. H. Shih, What we can learn about single photons in a two-photon interference experiment, Phys. Rev. A **57**, 567 (1998).

[42] M. A. Sagioro, C. Olindo, C. H. Monken, and S. Pádua, Time control of two-photon interference, Phys. Rev. A **69**, 053817 (2004).

[43] C. Olindo, M. A. Sagioro, C. H. Monken, S. Pádua, and A. Delgado, Hong-Ou-Mandel interferometer with cavities: Theory, Phys. Rev. A **73**, 043806 (2006).

[44] C. Olindo, M. A. Sagioro, S. Pádua, and C. H. Monken, Erasing

[45] nonlocal like two photon interference, Opt. Commun. **357**, 58 (2015).

[45] A. F. Abouraddy, M. B. Nasr, B. E. A. Saleh, A. V. Sergienko, and M. C. Teich, Quantum-optical coherence tomography with dispersion cancellation, Phys. Rev. A **65**, 053817 (2002).

[46] M. B. Nasr, B. E. A. Saleh, A. V. Sergienko, and M. C. Teich, Demonstration of Dispersion-Canceled Quantum-Optical Coherence Tomography, Phys. Rev. Lett. **91**, 083601 (2003).

[47] See Supplemental Material at http://link.aps.org/supplemental/10.1103/PhysRevResearch.5.L022005 for (I) the extended theoretical model, (II) rotation speed calibration, and (III) histogram of measurements.

[48] D. M. Shupe, Thermally induced nonreciprocity in the fiber-optic interferometer, Appl. Opt. **19**, 654 (1980).

[49] D. E. Bruschi, I. Fuentes, and J. Louko, Voyage to Alpha Centauri: Entanglement degradation of cavity modes due to motion, Phys. Rev. D **85**, 061701(R) (2012).

[50] N. Friis, D. E. Bruschi, J. Louko, and I. Fuentes, Motion generates entanglement, Phys. Rev. D **85**, 081701(R) (2012).

[51] P. M. Alsing and I. Fuentes, Observer dependent entanglement, Class. Quantum Grav. **29**, 224001 (2012).

[52] M. Cromb, S. Restuccia, G. M. Gibson, M. Toroš, M. J. Padgett, and D. Faccio, Mechanical rotation modifies the manifestation of photon entanglement: Dataset, Enlighten Research Data 1411 (2023).